JACS
JOURNAL OF THE AMERICAN CHEMICAL SOCIETY
Article
pubs.acs.org/JACS

Fragmentation Energetics of Clusters Relevant to Atmospheric New Particle Formation

Bryan R. Bzdek,[†] Joseph W. DePalma,[†] Douglas P. Ridge,[†] Julia Laskin,[‡] and Murray V. Johnston*,[†]

[†]Department of Chemistry and Biochemistry, University of Delaware, Newark, Delaware 19716, United States

[‡]Chemical and Material Sciences Division, Pacific Northwest National Laboratory, P.O. Box 999, K8-88, Richland, Washington 99352, United States

Supporting Information

ABSTRACT: The exact mechanisms by which small clusters form and grow in the atmosphere are poorly understood, but this process may significantly impact cloud condensation nuclei number concentrations and global climate. Sulfuric acid is the key chemical component to new particle formation (NPF), but basic species such as ammonia are also important. Few laboratory experiments address the kinetics or thermodynamics of acid and base incorporation into small clusters. This work utilizes a Fourier transform ion cyclotron resonance mass spectrometer equipped with surface-induced dissociation to investigate time- and collision-energy-resolved fragmentation of positively charged ammonium bisulfate clusters. Critical energies for dissociation are obtained from Rice−Ramsperger−Kassel−Marcus/quasi-equilibrium theory modeling of the experimental data and are compared to quantum chemical calculations of the thermodynamics of cluster dissociation. Fragmentation of ammonium bisulfate clusters occurs by two pathways: (1) a two-step pathway whereby the cluster sequentially loses ammonia followed by sulfuric acid and (2) a one-step pathway whereby the cluster loses an ammonium bisulfate molecule. Experimental critical energies for loss of an ammonia molecule and loss of an ammonium bisulfate molecule are higher than the thermodynamic values. If cluster growth is considered the reverse of cluster fragmentation, these results require the presence of an activation barrier to describe the incorporation of ammonia into small acidic clusters and suggest that kinetically (i.e., diffusion) limited growth should not be assumed. An important corollary is that models of atmospheric NPF should be revised to consider activation barriers to individual chemical steps along the growth pathway.

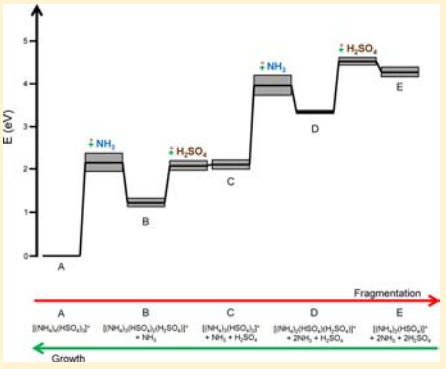

INTRODUCTION

The formation and growth of particles from gaseous precursors is an important and ubiquitous atmospheric process.[1,2] Particles arising from new particle formation (NPF) can ultimately serve as cloud condensation nuclei (CCN)[3,4] and in fact may constitute a substantial fraction of CCN.[5,6] When serving as CCN, these particles may impact precipitation patterns[7] and climate[8] by altering cloud albedo.[9,10] Despite its potential atmospheric importance, the chemical mechanisms governing NPF are not well understood, mainly because the early stages of particle formation and growth are difficult to study experimentally.[2,11−14]

Sulfuric acid is a key chemical species for NPF, as the nucleation rate in both field and laboratory measurements usually is proportional to the gas-phase sulfuric acid concentration.[15−19] However, measured ambient particle growth rates frequently cannot be explained solely by sulfuric acid condensation onto particles.[18−25] Experimental and theoretical studies of nucleation have found a substantial effect of basic species on particle formation rates.[26−32] As a result, small nucleating clusters are thought to be composed primarily of sulfuric acid,[17,33−36] water, and ammonia[33,37−40] or amines.[26,30,31,41−43] Organic species may also contribute to ambient NPF.[44−46] For nucleated particles to grow into the size range where they may serve as CCN, their growth rate must be substantially higher than their loss rate due to coagulation.[47] Because basic species are of critical importance to both nucleation and growth, a fundamental chemical and physical understanding of the mechanisms by which bases can incorporate into growing clusters is required.

The most convenient method to study small clusters experimentally is by mass spectrometry. Indeed, several studies have examined the kinetics and energetics of clusters that may serve as precursors to nucleation.[48−53] The majority of these studies examined cluster energetics by thermal dissociation in an ion trap. Recent experimental work on positively and negatively charged ammonium bisulfate clusters has suggested that cluster growth proceeds by an ammonium bisulfate coordinate (i.e., growth by 1:1 addition of H_2SO_4 and NH_3).[27,51] In our group, we have rigorously investigated the kinetics and thermodynamics of amine−ammonia exchange in small clusters using Fourier transform ion cyclotron resonance mass spectrometry (FTICR-MS) as well as computational

Received: December 27, 2012
Published: February 1, 2013

   dx.doi.org/10.1021/ja3124509 | J. Am. Chem. Soc. 2013, 135, 3276−3285

chemistry and have found that amines can displace ammonia in these clusters with nearly 100% reaction probability.[54−58] We also found that base can neutralize acidic clusters but at much lower reaction probabilities than displacement.[55−57] Although a portion of nonunity reaction probabilities could be explained by less than 100% coverage of the cluster surface with sulfuric acid, the reaction probabilities for ammonia addition were generally observed to be orders of magnitude below unity ($<10^{-2}$),[55−57] which suggests other factors should be explored to explain this observation. As such, these previous experiments did not fully reveal the mechanisms by which base can incorporate into a growing cluster or why base incorporation into acidic clusters has a low reaction probability.

In this work, we utilize FTICR-MS equipped with surface-induced dissociation (SID)[59] to study the fragmentation kinetics and energetics of positively charged ammonium bisulfate clusters. Experimental results are modeled using a Rice−Ramsperger−Kassel−Marcus/quasi-equilibrium theory (RRKM/QET) formalism to determine the fragmentation energetics.[60,61] We then compare the experimental fragmentation energetics to computationally derived and experimentally determined thermodynamic values to infer cluster growth mechanisms, as cluster growth can be considered the reverse of fragmentation. The results indicate that an activation barrier exists for the incorporation of ammonia and ammonium bisulfate into growing molecular clusters. Therefore, the growth of small clusters in the ammonia−sulfuric acid system should not be a kinetically (i.e., diffusion) limited process. These results imply that models of NPF should be revised to resolve individual chemical steps and consider the possibility of activation barriers to individual steps along the growth pathway.

EXPERIMENTAL SECTION

SID Experiments. SID experiments were conducted using a specially fabricated 6T FTICR-MS described in detail elsewhere.[59] A 5 mM ammonium sulfate (Sigma−Aldrich) solution in 50:50 water:-methanol was electrosprayed in the positive mode at atmospheric pressure to produce positively charged ammonium bisulfate clusters of the form $[(NH_4)_x(HSO_4)_{x-1}]^+$. These charged clusters were transferred into the vacuum system via an electrodynamic ion funnel.[62] Two quadrupoles following the ion funnel provide collisional focusing and mass selection of the ion of interest. Because the charged clusters studied in this experiment are metastable, mass selection of a particular cluster of interest was accomplished by setting the mass-selecting quadrupole to pass a cluster larger than the desired cluster.[55] The cluster selected by the quadrupole then decomposes in the octopole, where the desired precursor ion is isolated. The identity of the precursor is confirmed by transferring the ions in the octopole to the ICR cell in the absence of a collision potential and obtaining a mass spectrum. In the SID sequence, mass-selected clusters were accumulated, extracted from the accumulation octopole, transferred into the ICR cell (which is offset at a selected collision potential), and allowed to collide with the SID target at the selected collision energy. The kinetic energy of the ions colliding with the surface is varied by adjusting the dc offset applied to the ICR cell. The SID target is introduced through a vacuum interlock assembly and is positioned at the rear trapping plate of the ICR cell. Scattered positive ions were captured by raising the potentials on the front and rear trapping plates at the conclusion of the transfer time. Time-resolved mass spectra were acquired by varying the delay between the gated trapping and the excitation/detection event (reaction delay). In this experiment, reaction delays of 1, 5, 10, and 50 ms were examined. Immediately following the reaction delay, ions were excited through a broadband chirp and detected. The collision energy was the potential applied to the rear trapping plate and the SID target relative to that applied to the accumulation octopole. The SID target was a 1-dodecanethiol self-assembled monolayer surface prepared on a single gold {111} crystal (Monocrystals, Richmond Heights, OH) using a standard procedure. The target was cleaned in an UV cleaner (Model 135500, Boekel Industries Inc., Feasterville, PA) for 10 min and allowed to stand in a 98% 1-dodecanethiol solution (Sigma-Aldrich) for 8−12 h. The target was removed from the thiol solution and ultrasonically washed in ethanol for 10 min to remove extra layers. A modular FTICR data acquisition system was used to control the voltages and timing of the ion source, transfer optics, and ion manipulations in the ICR cell.[63,64] Survival curves and time-resolved fragmentation efficiency curves (TFECs) were constructed from experimental mass spectra by plotting the relative abundance of the precursor ion and its fragments as a function of collision energy at each reaction delay.

RRKM Modeling. Survival curves and TFECs were modeled using an RRKM/QET formalism described previously.[60,61] Briefly, the microcanonical rate coefficient $k(E)$ is calculated using the microcanonical RRKM/QET expression:

$$k(E) = \frac{\sigma W^{\ddagger}(E - E_0)}{h\rho(E)} \tag{1}$$

where $\rho(E)$ is the density of states of the reactant, $W^{\ddagger}(E - E_0)$ is the sum of states of the transition state, E_0 is the critical energy, h is Planck's constant, and σ is the reaction path degeneracy. The breakdown graph, a collection of breakdown curves (BDCs) representing the fragmentation probability of the precursor ion into a particular reaction channel as a function of the internal energy of the precursor ion (E) and the reaction delay (t_r), was calculated using the appropriate equations of formal kinetics derived for a particular reaction scheme. Because of the long reaction delay times involved in these experiments, radiative cooling of the excited ions was incorporated into the kinetics scheme.[65]

The internal energy deposition function was described by the following analytical expression:[60,61]

$$P(E, E_{coll}) = \frac{1}{C}(E - \Delta)^l \exp\left(-\frac{(E - \Delta)}{f(E_{coll})}\right) \tag{2}$$

where l and Δ are parameters obtained from reference ions, $C = \Gamma(l + 1)[f(E_{coll})]^{l+1}$ is a normalization factor, and $f(E_{coll})$ has the form:

$$f(E_{coll}) = A_2 E_{coll}^{\ 2} + A_1 E_{coll} + E_{th}/(l + 1) \tag{3}$$

where A_1 and A_2 are parameters obtained from reference ions, E_{th} is the thermal energy of the ensemble of ions prior to ion activation, and E_{coll} is the collision energy.

The normalized signal intensity for a particular reaction channel is given by:

$$I_i(E_{coll}) = \int_0^{\infty} BDC_i(E, t_r)P(E, E_{coll})\, dE \tag{4}$$

Calculated TFECs were constructed using this described procedure and then were compared to the experimental data. The same energy deposition function was used for all reaction delays, and the fitting parameters were varied until the best fit to the experimental curves was obtained. The model also considers energy partitioning into the neutral fragments.[61,66] The fitting parameters included critical energies (E_0) and activation entropies ($\Delta S^{\ddagger}$) for all reaction channels. The parameters l, Δ, A_1, and A_2 characterizing the energy deposition function (eqs 2 and 3) were determined by fitting the experimental survival curves for protonated leucine enkephalin (YGGFL) and its derivative (RYGGFL), for which the dissociation parameters are already known.[67,68] In order to ensure fits did not converge to local minima, each model was fit using random starting points for E_0 and $\Delta S^{\ddagger}$. Additionally, we systematically removed experimental data points in order to examine the effect on the RRKM/QET model fits. The purpose of doing this was to elucidate the effect of experimental scatter on the resulting model fits. For instance, in one iteration of this exercise, every fifth experimental data point was removed. Although this exercise resulted in a broader range of E_0 values (which are reported in the tables), the conclusions obtained from the RRKM/

dx.doi.org/10.1021/ja3124509 | J. Am. Chem. Soc. 2013, 135, 3276−3285

QET model fits do not change. Parameters were also individually fixed to expected thermodynamic values while the rest were varied in order to ensure that certain thermodynamic values (see below) could or could not accurately explain the experimental data. Finally, the data were modeled such that pathways present in the $[(NH_4)_6(HSO_4)_5]^+$ SID experiment as well as in the $[(NH_4)_5(HSO_4)_4]^+$ SID experiment were included in the modeling of the $[(NH_4)_5(HSO_4)_4]^+$ SID experiment. In this manner, redundant pathways were analyzed by two different models. E_0 values for identical fragmentation pathways were consistent between the two models.

Computational Procedure. Structures and energetics of the precursor and product ions discussed in this work were calculated using a method previously described.[58] Briefly, initial positively charged cluster geometries were constructed from individual optimized molecules of ammonia and sulfuric acid and then optimized to a minimum at the AM1 level of theory[69] using the HyperChem 8.0.8 GUI-based molecular modeling package.[70] Monte Carlo conformational searches were performed in the NVT ensemble using HyperChem 8.0.8 to generate a test set of configurations for further optimizations. Of the 4000 structures generated for every cluster studied, the 10 most energetically favorable structures were selected for full optimization with AM1. The most stable structure for a given cluster from the AM1/Monte Carlo method was further optimized with the PW91 functional[71,72] using the 6-31++G(d,p) basis set as implemented in Gaussian 09 (version C.01).[73] For selected clusters, further energy refinement was performed using MP2[74] with the aug-cc-pVTZ basis set[75] at the PW91/6-31++G(d,p) geometries for each optimized cluster with the zero-point corrections from PW91 applied. We note that the computational values we derive for these clusters are consistent with experimental thermodynamic values determined by Froyd and Lovejoy[51] to which we also compare our SID experimental values. Molecular coordinates and raw energy data are provided in the Supporting Information.

RESULTS AND DISCUSSION

Electrospray ionization of an ammonium sulfate solution in the positive mode produces an array of positively charged clusters predominantly in the form $[(NH_4)_x(HSO_4)_{x-1}]^+$.[57] In this study, the fragmentation energetics of two specific ammonium bisulfate clusters, $[(NH_4)_6(HSO_4)_5]^+$ and $[(NH_4)_5(HSO_4)_4]^+$, were studied by energy-resolved FTICR-MS-SID. Each cluster was isolated and then impacted against a surface at precisely known collision energies. The resulting fragmentation patterns were modeled using an RRKM/QET formalism to determine threshold energies for dissociation.

SID of $[(NH_4)_6(HSO_4)_5]^+$. Scheme 1 presents the fragmentation pathway for $[(NH_4)_6(HSO_4)_5]^+$. Upon collision

Scheme 1

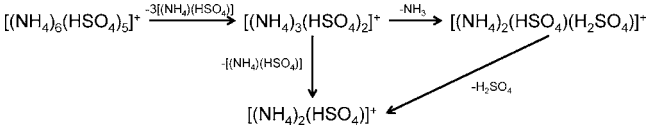

with the surface, this cluster immediately and completely fragments to $[(NH_4)_3(HSO_4)_2]^+$. Then, as the collision energy increases, two subsequent fragmentation pathways are observed. The first is a stepwise pathway whereby $[(NH_4)_3(HSO_4)_2]^+$ loses an ammonia molecule to form the acidic cluster $[(NH_4)_2(HSO_4)(H_2SO_4)]^+$ and then loses a sulfuric acid molecule to form $[(NH_4)_2(HSO_4)]^+$. The second pathway is a one-step loss of an ammonium bisulfate molecule from $[(NH_4)_3(HSO_4)_2]^+$ to form $[(NH_4)_2(HSO_4)]^+$. These two distinct fragmentation pathways have been observed in fragmentation studies of other salt clusters.[76,77] We note that a stepwise fragmentation pathway whereby sulfuric acid loss occurs first followed by ammonia loss was not observed. Such a pathway would result in the formation of $[(NH_4)_2(HSO_4)(NH_3)]^+$, which has a unique mass-to-charge ratio that was not observed in the mass spectra.

Figure 1 presents the TFECs for SID of $[(NH_4)_6(HSO_4)_5]^+$ (given by the symbols) as a function of SID collision energy and reaction delay. As mentioned previously, although the $[(NH_4)_6(HSO_4)_5]^+$ cluster was isolated at the start of the experiment, upon SID, it immediately and completely fragments to $[(NH_4)_3(HSO_4)_2]^+$. Therefore, the relative abundance of $[(NH_4)_6(HSO_4)_5]^+$ is zero even at low collision energy. $[(NH_4)_3(HSO_4)_2]^+$ is at 100% relative abundance at collision energies below 70 eV, but with increasing collision energy, it fragments and eventually approaches zero relative abundance at high collision energy. Meanwhile, the final product ion, $[(NH_4)_2(HSO_4)]^+$, initially has no abundance, but with increasing collision energy (E_{coll} > 90 eV) increases in relative abundance and ultimately constitutes nearly 100% of the total ion signal at high collision energies. The more acidic product, $[(NH_4)_2(HSO_4)(H_2SO_4)]^+$, which is the intermediate product in the two-step fragmentation pathway and represents the loss of an ammonia molecule from $[(NH_4)_3(HSO_4)_2]^+$, increases in abundance with increasing collision energy beginning around E_{coll} = 70 eV, reaches a maximum relative abundance at E_{coll} = 90−100 eV, and then decreases at higher collision energies as the cluster fragments by loss of a sulfuric acid molecule to form the final product ion, $[(NH_4)_2(HSO_4)]^+$.

Fits to RRKM/QET modeling at each reaction delay are given by the lines in Figure 1. The model was developed using the appropriate equations of formal kinetics derived for the reaction described by Scheme 1. Although there is some scatter in the experimental data, the fits reasonably reproduce the experimental results. The RRKM/QET model used incorporates only E_0 and $\Delta S^{\ddagger}$ as adjustable parameters. As previously mentioned in the Experimental Section, in order to ensure that scatter among the experimental data did not bias the RRKM/QET model fit, we systematically removed data points and examined the effects on the model fits. The E_0 and $\Delta S^{\ddagger}$ values did not change significantly. Results from all fits are included in the tables. Table 1 presents the results of the RRKM/QET model fit to the experimental data for $[(NH_4)_6(HSO_4)_5]^+$ as well as thermodynamic values obtained from computational modeling and an experimental study of the precursor and product ions. Because the initial fragmentation of $[(NH_4)_6(HSO_4)_5]^+$ to $[(NH_4)_3(HSO_4)_2]^+$ was not observed experimentally, we do not interpret the model results for this step, since presumably, the precursor ion was "hot" (i.e., contained a high, nonthermal initial internal energy distribution). The data in Table 1 suggest several interesting conclusions. First, the loss of ammonia from $[(NH_4)_3(HSO_4)_2]^+$ to form $[(NH_4)_2(HSO_4)(H_2SO_4)]^+$ has an experimental E_0 value in the range 1.80 ± 0.23 eV whereas the thermodynamic value is much lower at 1.15−1.20 eV. Similarly, for the step involving loss of an ammonium bisulfate molecule from $[(NH_4)_3(HSO_4)_2]^+$ to form $[(NH_4)_2(HSO_4)]^+$, the experimental E_0 value is 1.85 ± 0.25 eV, whereas the thermodynamic E_0 value is again much lower at 1.20−1.42 eV. These results suggest a reverse activation barrier exists for ammonia and ammonium bisulfate molecule losses. Furthermore, the $\Delta S^{\ddagger}$ values observed for these reaction pathways are close to 0 eu within experimental error (the model fit is relatively insensitive to the magnitude of $\Delta S^{\ddagger}$), indicating that

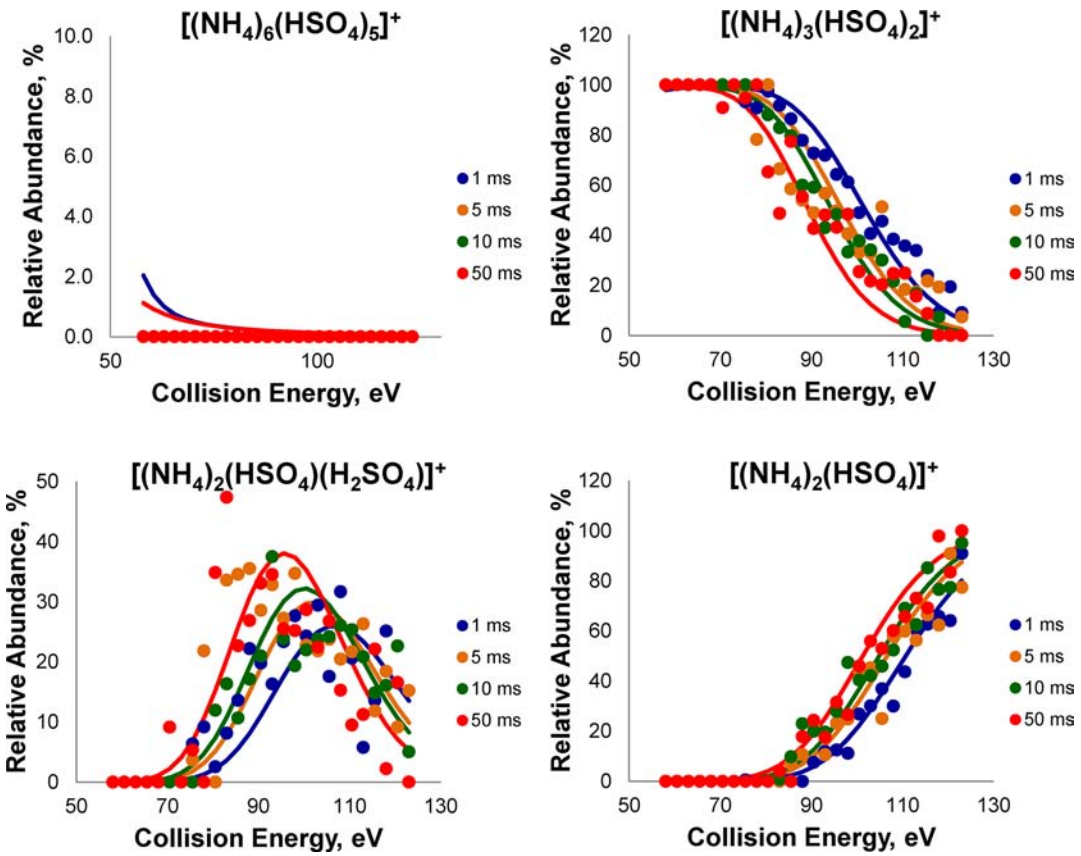

Figure 1. Time- and collision-energy-resolved fragmentation efficiency curves (symbols) and RRKM/QET model fits (lines) for SID of $[(NH_4)_6(HSO_4)_5]^+$. Note the different *y* axis scales.

Table 1. Summary of RRKM/QET Model Fits to Experimental Data and Thermodynamic Values for Fragmentation of $[(NH_4)_6(HSO_4)_5]^+$

fragmentation step	$[(NH_4)_6(HSO_4)_5]^+ \rightarrow [(NH_4)_3(HSO_4)_2]^+$	$[(NH_4)_3(HSO_4)_2]^+ \rightarrow [(NH_4)_2(HSO_4)(H_2SO_4)]^+$	$[(NH_4)_3(HSO_4)_2]^+ \rightarrow [(NH_4)_2(HSO_4)]^+$	$[(NH_4)_2(HSO_4)(H_2SO_4)]^+ \rightarrow [(NH_4)_2(HSO_4)]^+$
neutral loss	$3[(NH_4)_3(HSO_4)_3]$	NH_3	$[(NH_4)(HSO_4)]$	H_2SO_4
E_0 (eV, this work)	1.57 ± 1.07	1.80 ± 0.23	1.85 ± 0.25	1.15 ± 0.09
E_0 (eV, PW91/6-31++G(d,p))[a]	3.81	1.15	1.20	0.84
E_0 (eV, MP2/aug-cc-pVTZ)[a]		1.18	1.42	1.00
E_0 (eV, exptl)[b]		1.20		1.05
$\Delta S^{\ddagger}$ (eu, this work)[c]	n.s.[d]	1.12 ± 6.23	0.78 ± 6.52	n.s.[d]

[a] $E_0 = E_{electronic} + E_{zero\ point}$. [b] Thermodynamic values from Froyd and Lovejoy.[51] [c] eu = entropy unit = cal·mol^{-1}·K^{-1}, at 450 K. $\Delta S^{\ddagger}$ had a wide range of values among the model fits. [d] n.s. = model fits are not sensitive to this parameter.

for the loss of ammonia and the loss of an ammonium bisulfate molecule the fragmentation proceeds through a relatively tight transition state. These findings are consistent with the presence of a reverse activation barrier for these fragmentation channels (i.e., a barrier to the association of the two fragments).

For sulfuric acid loss from $[(NH_4)_2(HSO_4)(H_2SO_4)]^+$, the experimental E_0 value is 1.15 ± 0.09, which is close to the thermodynamic value (0.84−1.05 eV), suggesting that little if any reverse activation barrier exists. The absence of a reverse activation barrier is consistent with previous work on the sulfuric acid dimer that suggests its formation is kinetically (i.e., diffusion) limited.[34,78] We note that the RRKM/QET formalism used to model the experimental results does not explicitly include a reverse activation barrier along this fragmentation pathway. In other words, the model does not account for the lower potential well between the ammonia loss and sulfuric acid loss steps. Including such an activation barrier would cause the model fit to be highly uncertain, since its accuracy would depend upon the energy partitioning description and the partitioning of the reverse activation barrier into vibrational excitation, neither of which is well-known. On the basis of the previous studies and the relatively good agreement between the experiment and theory, we assume that only a very small fraction of the reverse activation barrier is partitioned into the vibrational degrees of freedom of the ionic fragment and that the rest is converted into kinetic energy.

SID of $[(NH_4)_5(HSO_4)_4]^+$. SID of the smaller $[(NH_4)_5(HSO_4)_4]^+$ cluster exhibited more complex fragmentation patterns. Scheme 2 presents the fragmentation pattern of $[(NH_4)_5(HSO_4)_4]^+$. First, the precursor ion fragmented to two

Scheme 2

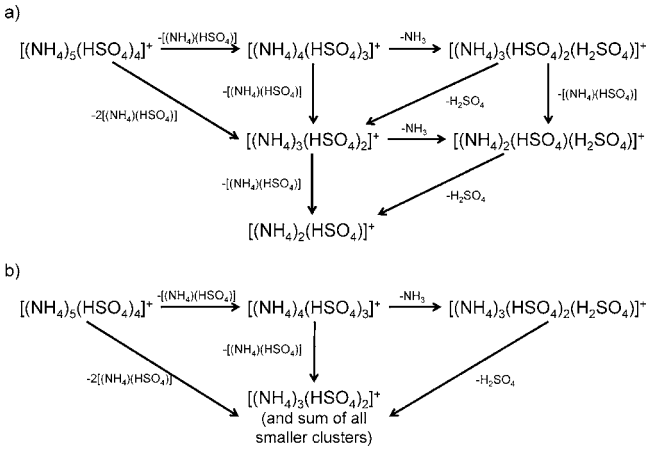

different product ions, $[(NH_4)_4(HSO_4)_3]^+$ and $[(NH_4)_3(HSO_4)_2]^+$. As a result, there are more steps involved in the fragmentation of this cluster than for $[(NH_4)_6(HSO_4)_5]^+$. The fragmentation of $[(NH_4)_5(HSO_4)_4]^+$ is described by Scheme 2a. $[(NH_4)_5(HSO_4)_4]^+$ fragments to $[(NH_4)_4(HSO_4)_3]^+$ and $[(NH_4)_3(HSO_4)_2]^+$. $[(NH_4)_4(HSO_4)_3]^+$ then can lose an ammonia molecule to form $[(NH_4)_3(HSO_4)_2(H_2SO_4)]^+$ and then a sulfuric acid molecule to form $[(NH_4)_3(HSO_4)_2]^+$, or it can fragment to $[(NH_4)_3(HSO_4)_2]^+$ in one step via loss of an ammonium bisulfate molecule. The $[(NH_4)_3(HSO_4)_2]^+$ cluster then fragments in the manner discussed in the previous section. Additionally, it is possible for $[(NH_4)_3(HSO_4)_2(H_2SO_4)]^+$ to fragment to $[(NH_4)_2(HSO_4)(H_2SO_4)]^+$ in one step by loss of an ammonium bisulfate molecule. In the RRKM/QET modeling of the fragmentation energetics, the fragmentation was considered in the manner described by Scheme 2b, where the signal for $[(NH_4)_3(HSO_4)_2]^+$ is summed with all smaller clusters, since the fragmentation as described by Scheme 2a was too complex to model. In this way, only five pathways are considered, most significantly the ammonia loss from $[(NH_4)_4(HSO_4)_3]^+$, the sulfuric acid loss from $[(NH_4)_3(HSO_4)_2(H_2SO_4)]^+$, and the ammonium bisulfate molecule loss from $[(NH_4)_4(HSO_4)_3]^+$.

Figure 2 presents the experimental TFECs and the fit to the RRKM/QET model using Scheme 2b to describe the fragmentation. Even at low collision energies, most of the $[(NH_4)_5(HSO_4)_4]^+$ cluster fragments to $[(NH_4)_4(HSO_4)_3]^+$ and $[(NH_4)_3(HSO_4)_2]^+$; however, there is still a small abundance of $[(NH_4)_5(HSO_4)_4]^+$. There is some abundance of $[(NH_4)_4(HSO_4)_3]^+$ that initially increases in intensity as the residual $[(NH_4)_5(HSO_4)_4]^+$ fragments but above E_{coll} = ~60 eV begins to lose intensity as it fragments to $[(NH_4)_3(HSO_4)_2(H_2SO_4)]^+$ and $[(NH_4)_3(HSO_4)_2]^+$. $[(NH_4)_3(HSO_4)_2(H_2SO_4)]^+$ increases from zero abundance due to fragmentation of $[(NH_4)_4(HSO_4)_3]^+$, reaches a maximum abundance around E_{coll} = 65 eV, and then decreases in abundance as it fragments to $[(NH_4)_3(HSO_4)_2]^+$ by loss of a sulfuric acid molecule. Finally, $[(NH_4)_3(HSO_4)_2]^+$ begins with a relatively large abundance and then increases to 100% abundance as larger clusters fragment. Again, despite some scatter in the experimental data and the complexity of the

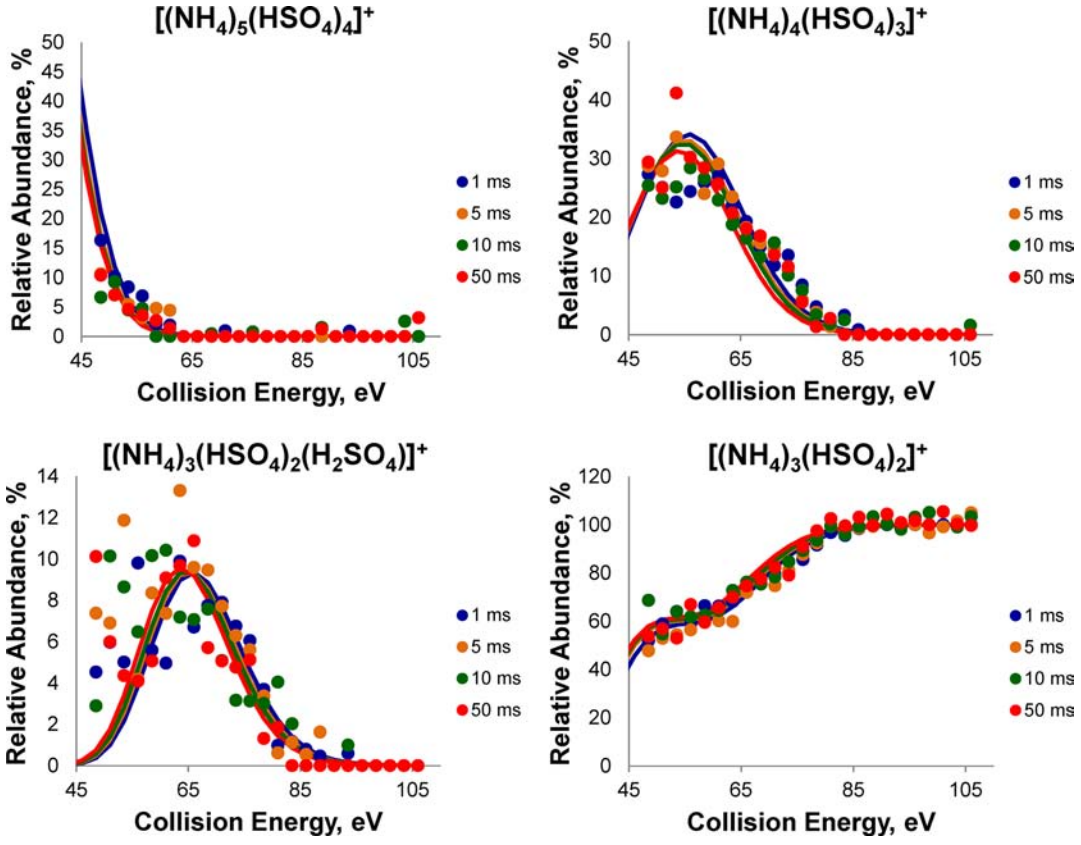

Figure 2. Time- and collision-energy-resolved fragmentation efficiency curves (symbols) and RRKM/QET model fits (lines) for SID of $[(NH_4)_5(HSO_4)_4]^+$. Note the different *y* axis scales.

dx.doi.org/10.1021/ja3124509 | J. Am. Chem. Soc. 2013, 135, 3276−3285

Table 2. Summary of RRKM/QET Model Fits to Experimental Data and Thermodynamic Values for Fragmentation of $[(NH_4)_5(HSO_4)_4]^+$

fragmentation step	$[(NH_4)_5(HSO_4)_4]^+ \rightarrow [(NH_4)_4(HSO_4)_3]^+$	$[(NH_4)_5(HSO_4)_4]^+ \rightarrow [(NH_4)_3(HSO_4)_2]^+$	$[(NH_4)_4(HSO_4)_3]^+ \rightarrow [(NH_4)_3(HSO_4)_2(H_2SO_4)]^+$	$[(NH_4)_4(HSO_4)_3]^+ \rightarrow [(NH_4)_3(HSO_4)_2]^+$	$[(NH_4)_3(HSO_4)_2(H_2SO_4)]^+ \rightarrow [(NH_4)_3(HSO_4)_2]^+$
neutral loss	$[(NH_4)\ (HSO_4)]$	$2[(NH_4)_2(HSO_4)_2]$	NH_3	$[(NH_4)\ (HSO_4)]$	H_2SO_4
E_0 (eV, this work)	1.87 ± 0.48	1.74 ± 0.49	2.13 ± 0.21	2.03 ± 0.31	0.84 ± 0.11
E_0 (eV, PW91/6-31++G(d,p))[a]	1.38	2.70	1.32	1.32	0.80
E_0 (eV, MP2/aug-cc-pVTZ)[a]			1.24	1.21	0.74
E_0 (eV, exptl)[b]			1.12		0.95
$\Delta S^{\ddagger}$ (eu, this work)[c]	≫0	≫0	≫0	≫0	≫0

[a] $E_0 = E_{electronic} + E_{zero\ point}$. [b] Thermodynamic values from Froyd and Lovejoy.[51] [c] eu = entropy unit = cal·mol^{-1}·K^{-1}, at 450 K. $\Delta S^{\ddagger}$ had a wide range of very positive values among the model fits.

fragmentation scheme, the RRKM/QET model captures the main fragmentation trends.

Table 2 gives RRKM/QET model fits to the experimental data for the SID of $[(NH_4)_5(HSO_4)_4]^+$ as well as thermodynamic values. Because the intensity of $[(NH_4)_5(HSO_4)_4]^+$ is so low even at low collision energy in the experiment, no interpretation of the fragmentations of this cluster to $[(NH_4)_4(HSO_4)_3]^+$ or $[(NH_4)_3(HSO_4)_2]^+$ is attempted. Loss of an ammonia molecule from $[(NH_4)_4(HSO_4)_3]^+$ requires an experimental E_0 value of 2.13 ± 0.21 eV, which is much higher than the thermodynamic value (1.12−1.32 eV). Similarly, the loss of the ammonium bisulfate molecule from $[(NH_4)_4(HSO_4)_3]^+$ requires 2.03 ± 0.31 eV, which is also higher than the thermodynamic value (1.21−1.32 eV). These observations suggest the presence of a reverse activation barrier in both of these cases. For the sulfuric acid loss from $[(NH_4)_3(HSO_4)_2(H_2SO_4)]^+$, the experimental E_0 value (0.84 ± 0.11 eV) is within the range of thermodynamic values (0.80−0.95 eV), suggesting that there is no reverse activation barrier. $\Delta S^{\ddagger}$ values were very high and variable for this cluster (always much greater than zero), which is a result of the reduced time dependence in the data set for this cluster.

It is notable that the same three pathways (ammonia loss, sulfuric acid loss, and ammonium bisulfate molecule loss) are observed for the fragmentation of both clusters. Additionally, E_0 values for the same pathway in each cluster are consistent. In both clusters, a reverse activation barrier is required to explain the ammonia and the ammonium bisulfate molecule loss pathways. The difference in $\Delta S^{\ddagger}$ for the ammonia and the ammonium bisulfate molecule losses from $[(NH_4)_3(HSO_4)_2]^+$ (where $\Delta S^{\ddagger}$ is near 0 eu) and from $[(NH_4)_4(HSO_4)_3]^+$ (where $\Delta S^{\ddagger}$ is much greater than 0 eu) suggests that, as cluster size increases, the transition state becomes less constrained.

Potential Energy Surfaces. SID of the two positively charged ammonium bisulfate clusters examined in this study suggests two unique pathways for cluster fragmentation. One is a two-step pathway whereby a cluster first loses an ammonia molecule and then loses a sulfuric acid molecule, whereas the other is a one-step pathway proceeding via the loss of an ammonium bisulfate molecule. RRKM/QET modeling of the experimental results and the electronic structure calculations provide information on the energetics and dynamics of these fragmentation channels.

Figure 3a presents a potential energy surface describing the stepwise ammonia and sulfuric acid losses. As discussed previously, the experimental E_0 values for the ammonia loss pathways are higher than the thermodynamic values. If one

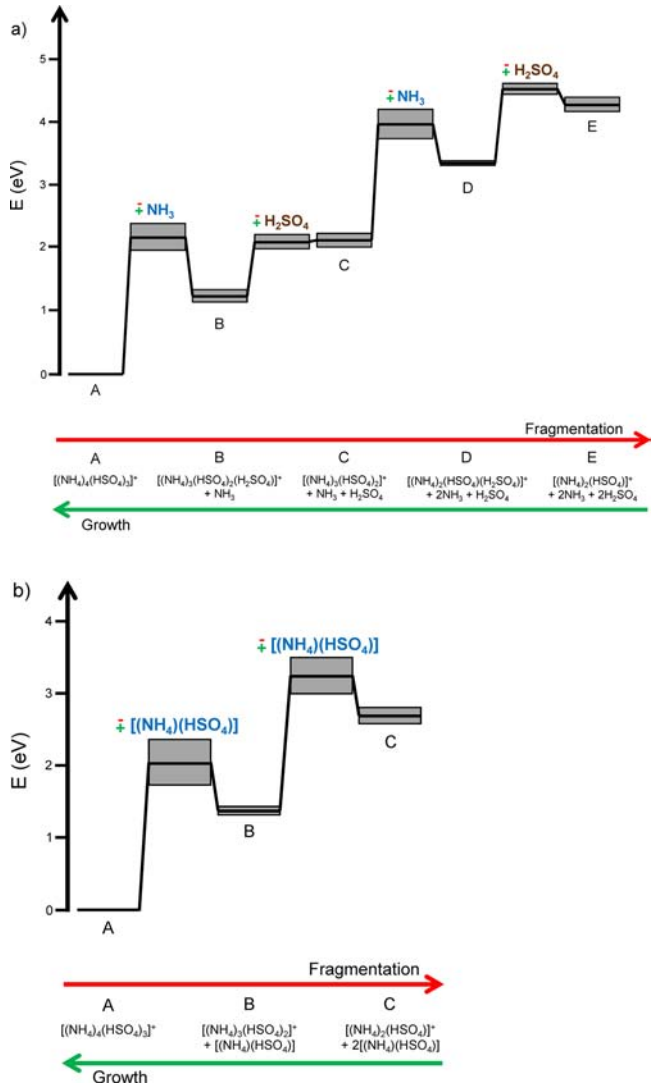

Figure 3. Potential energy surfaces for the (a) two-step sequential ammonia−sulfuric acid loss pathway and (b) one-step ammonium bisulfate molecule loss from pathway. Lines show the average value. Gray boxes show ranges. Letters (A−E) indicate thermodynamic values. In the absence of reverse activation barriers, the fragmentation process would begin from the energy level marked A to the level marked B, etc. Between these levels are shown barrier heights marked with the outgoing/incoming molecule.

dx.doi.org/10.1021/ja3124509 | J. Am. Chem. Soc. 2013, 135, 3276−3285

were to consider cluster growth to be the reverse of cluster fragmentation, ammonia addition to neutralize the sulfuric acid must overcome an activation barrier, whereas sulfuric acid addition is close to barrierless. The presence of an activation barrier probably arises because cluster binding is strong and is mostly due to electrostatic interactions.[58] As a result, when the ammonia molecule interacts with a cluster-bound sulfuric acid molecule to form ionic ammonium bisulfate within the cluster, a rearrangement of the electrostatic interactions, including a charge separation between the two species, must occur. Such a rearrangement of the electrostatic interactions in the cluster structure is analogous to surface reconstruction in surface science.

Figure 3b presents a potential energy surface describing the one-step fragmentation pathway, whereby the cluster loses an ammonium bisulfate molecule. For this pathway, the experimental E_0 values were higher than the thermodynamic value determined by computational chemistry. If one were to consider the reverse pathway, cluster growth by accretion of ammonium bisulfate molecules, these results suggest that, to add an ammonium bisulfate molecule to the growing cluster, one must overcome an activation barrier. The presence of a barrier to the addition of the ammonium bisulfate molecule suggests that a substantial rearrangement of the cluster structure must occur in order for the addition to occur. This explanation is in qualitative agreement with structural modeling of these clusters performed previously by our group, as the structure and electrostatic interactions change significantly as the cluster grows from $[(NH_4)_2(HSO_4)]^+$ to $[(NH_4)_3(HSO_4)_2]^+$ to $[(NH_4)_4(HSO_4)_3]^+$.[58] However, this pathway may not be atmospherically relevant, as the ambient concentration of the ammonium bisulfate molecule is expected to be very low.[79] The activation barrier heights presented in this work are very high, and we caution against a quantitative interpretation of the barrier height. The activation barrier height should be considered qualitative rather than quantitative because we do not fully consider energy partitioning in its determination.

Atmospheric Implications. In the atmosphere, nucleating clusters are thought to be composed of sulfuric acid, ammonia, amines, and water. However, the early steps of NPF are poorly understood, especially in terms of the chemical mechanisms for cluster growth. Nonetheless, laboratory studies have found that the growth of sulfuric acid–ammonia clusters proceeds by an ammonium bisulfate coordinate (1:1 ratio of H_2SO_4:NH_3), though whether this growth occurs in one step or two steps was not rigorously investigated.[27,51]

The implications concerning the existence of an activation barrier to sulfuric acid neutralization by ammonia may be significant with respect to cluster distributions to be expected in the atmosphere and in laboratory experiments that mimic atmospheric conditions. In the atmosphere, ammonia concentrations are typically 2 orders of magnitude higher than sulfuric acid concentrations.[80] As a result, the height of the activation barrier and the ambient concentrations will dictate the extent of cluster neutralization. Figure 4 illustrates three possible scenarios where the reaction kinetics have been modeled taking into account the differences in atmospheric concentrations of sulfuric acid and ammonia as well as the height of the activation barrier for ammonia addition to an acidic cluster. Sulfuric acid uptake is assumed to be barrierless in these examples. The barrier height was used to calculate an expected uptake coefficient (γ_{NH_3}) by:

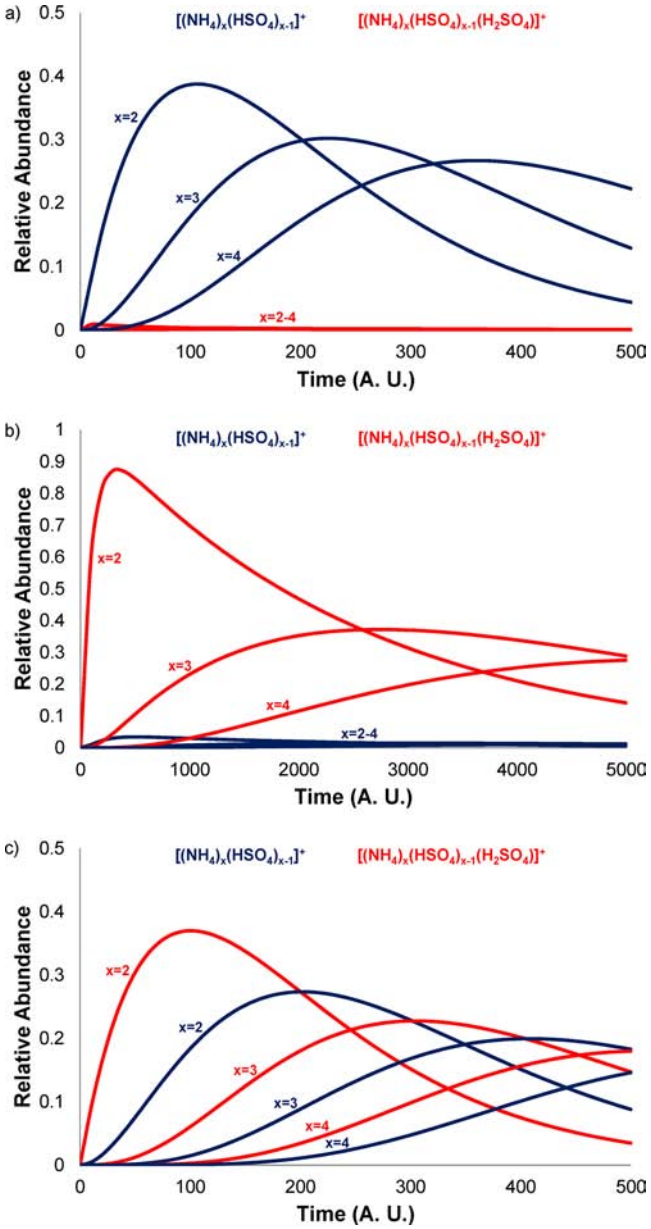

Figure 4. Modeled cluster distributions assuming $[NH_3] = 100 \times [H_2SO_4]$, $\gamma_{H_2SO_4} = 1$, and (a) $E_{RAB} = 0$ eV, (b) $E_{RAB} = 0.2$ eV, and (c) $E_{RAB} = 0.1$ eV for ammonia addition. Blue lines are clusters neutralized to bisulfate; red lines are acidic clusters (one un-neutralized sulfuric acid molecule). Each line indicates sequential values of x beginning with an arbitrary initial cluster ($x = 2$).

$$\gamma_{NH_3} = e^{-E_{RAB}/kT} \quad (5)$$

where k is the Boltzmann constant and T is the temperature.

Figure 4a illustrates a limiting scenario where $E_{RAB} = 0$ eV ($\gamma_{NH_3} = 1$). In this case, both sulfuric acid addition and the subsequent ammonia addition occur with unit probability. However, because the ammonia concentration is typically 2 orders of magnitude higher than that of sulfuric acid, the apparent rate for ammonia addition would be 2 orders of magnitude higher than the rate of sulfuric acid addition. As illustrated in Figure 4a, this scenario results in neutralized clusters (blue lines) dominating over acidic clusters (red lines).

dx.doi.org/10.1021/ja3124509 | J. Am. Chem. Soc. 2013, 135, 3276–3285

Figure 4b illustrates a second limiting scenario where E_{RAB} = 0.2 eV ($\gamma_{NH_3} = 10^{-4}$). In this case, uptake of ammonia is 4 orders of magnitude slower than uptake of sulfuric acid. Despite the higher concentration of ammonia, the rate of ammonia addition will still be 2 orders of magnitude slower than that of sulfuric acid addition. As shown in Figure 4b, the result is that acidic clusters dominate over neutralized clusters. Also significant for this limiting scenario is the much longer time scale to cluster growth, as the neutralization step is very slow.

Figure 4c presents an intermediate scenario where E_{RAB} = 0.1 eV ($\gamma_{NH_3} = 10^{-2}$). In this case, although the uptake coefficient for ammonia is 2 orders of magnitude lower than that for sulfuric acid, the larger abundance of ammonia can overcome the kinetic barrier to addition. As a result, the relative rates for sulfuric acid and ammonia addition are the same. As shown in Figure 4c, the result is that both acidic and neutralized clusters have significant abundance. Such a scenario is in qualitative agreement with a recent chamber study examining NPF with the ammonia–sulfuric acid system.[27] The above analysis illustrates the concept that the cluster distribution is strongly dependent on E_{RAB} even though all individual steps are thermodynamically strongly favorable.[51,58]

CONCLUSIONS

In this work, an RRKM/QET model was applied to time- and collision-energy-resolved fragmentation by SID of positively charged ammonium bisulfate clusters. The experimental results indicate that two distinct fragmentation pathways exist: (1) a two-step fragmentation whereby ammonia and sulfuric acid are sequentially lost from the cluster and (2) a one-step fragmentation whereby an ammonium bisulfate molecule is lost from the cluster. RRKM/QET modeling of the experimental SID data indicates that the critical energies for loss of an ammonia molecule and loss of an ammonium bisulfate molecule from a cluster are larger than the thermodynamic values. If one were to consider cluster growth to be the reverse of cluster fragmentation, the results suggest that an activation barrier must be overcome in order to neutralize sulfuric acid in a small cluster with ammonia. The implication therefore is that the reaction probability for neutralization by ammonia in an acidic cluster will be much less than unity though the observed distribution and composition of clusters will be strongly dependent on the barrier height and relative concentrations of the gaseous sulfuric acid and ammonia. Our results also suggest an activation barrier exists to the addition of the ammonium bisulfate molecule. The presence of an activation barrier to ammonia incorporation in principle could be tested experimentally in a nucleation experiment if the molecular ions are monitored and the ammonia concentration is varied. These results indicate that cluster growth in the ammonia–sulfuric acid system is probably not kinetically limited due to the presence of activation barriers along the potential energy surface. Models of atmospheric particle nucleation and growth typically focus on free energy differences among clusters of different sizes and do not consider activation barriers to growth processes in much, if any, detail.[2,81−83] The results presented here suggest that it may be appropriate to incorporate activation barrier into models of NPF. Indeed, these observations may be broadly applicable to studies of heterogeneous nanoparticle/cluster growth, as the concept of activation barriers along individual chemical steps may be important to consider in understanding such processes.

There are some important limitations to this work that will require further investigation. The activation barrier height, the cluster polarity effects, and the role of water are not quantified. Additionally, the cluster size dependence of the barrier is not well defined. An important question to address is whether an activation barrier can exist in larger clusters and whether that may affect observed kinetics. Finally, this work only addresses ammonium bisulfate clusters. Whether amines would exhibit similar behavior as ammonia or could lower the activation barrier to sulfuric acid neutralization and thereby facilitate higher cluster growth rates is an open question. A reduced activation barrier associated with amines may help to explain the enhanced nucleation rates observed in laboratory studies of sulfuric acid–amine nucleation.

ASSOCIATED CONTENT

Supporting Information

Molecular coordinates and raw energy data from the computational calculations. This material is available free of charge via the Internet at http://pubs.acs.org.

AUTHOR INFORMATION

Corresponding Author

mvj@udel.edu

Notes

The authors declare no competing financial interest.

ACKNOWLEDGMENTS

This work was supported by National Science Foundation (NSF) grant no. CHE-1110554 and NSF/XSEDE supercomputing resources (grant TG-ATM100041). J.L. acknowledges support from the U.S. Department of Energy's (DOE) Office of Basic Energy Sciences, Division of Chemical Sciences, Geosciences and Biosciences. The SID experiments were performed using EMSL, a national scientific user facility sponsored by the DOE's Office of Biological and Environmental Research and located at Pacific Northwest National Laboratory. B.R.B. acknowledges graduate fellowships from the University of Delaware Center for Critical Zone Research; American Chemical Society, Division of Analytical Chemistry Fellowship, sponsored by the Society for Analytical Chemists of Pittsburgh; and a STAR Graduate Fellowship (FP-91731501) awarded by the U.S. Environmental Protection Agency.

REFERENCES

(1) Kulmala, M.; Vehkamaki, H.; Petaja, T.; Dal Maso, M.; Lauri, A.; Kerminen, V. M.; Birmili, W.; McMurry, P. H. *J. Aerosol Sci.* **2004**, *35*, 143−176.

(2) Zhang, R.; Khalizov, A.; Wang, L.; Hu, M.; Xu, W. *Chem. Rev.* **2012**, *112*, 1957−2011.

(3) Kerminen, V. M.; Lihavainen, H.; Komppula, M.; Viisanen, Y.; Kulmala, M. *Geophys. Res. Lett.* **2005**, *32*, L14803.

(4) Wiedensohler, A.; Cheng, Y. F.; Nowak, A.; Wehner, B.; Achtert, P.; Berghof, M.; Birmili, W.; Wu, Z. J.; Hu, M.; Zhu, T.; Takegawa, N.; Kita, K.; Kondo, Y.; Lou, S. R.; Hofzumahaus, A.; Holland, F.; Wahner, A.; Gunthe, S. S.; Rose, D.; Su, H.; Poschl, U. *J. Geophys. Res.: Atmos.* **2009**, *114*, D00G08.

(5) Kuang, C.; McMurry, P. H.; McCormick, A. V. *Geophys. Res. Lett.* **2009**, *36*, L09822.

(6) Merikanto, J.; Spracklen, D. V.; Mann, G. W.; Pickering, S. J.; Carslaw, K. S. *Atmos. Chem. Phys.* **2009**, *9*, 8601−8616.

(7) Lee, S. S.; Feingold, G. *Geophys. Res. Lett.* **2010**, *37*, L23806.

(8) Rosenfeld, D.; Lohmann, U.; Raga, G. B.; O'Dowd, C. D.; Kulmala, M.; Fuzzi, S.; Reissell, A.; Andreae, M. O. *Science* **2008**, *321*, 1309−1313.
(9) Charlson, R. J.; Schwartz, S. E.; Hales, J. M.; Cess, R. D.; Coakley, J. A.; Hansen, J. E.; Hofmann, D. J. *Science* **1992**, *255*, 423−430.
(10) Lohmann, U.; Feichter, J. *Atmos. Chem. Phys.* **2005**, *5*, 715−737.
(11) Bzdek, B. R.; Johnston, M. V. *Anal. Chem.* **2010**, *82*, 7871−7878.
(12) Bzdek, B. R.; Pennington, M. R.; Johnston, M. V. *J. Aerosol Sci.* **2012**, *52*, 109−120.
(13) Laskin, A.; Laskin, J.; Nizkorodov, S. A. *Environ. Chem.* **2012**, *9*, 163−189.
(14) Riipinen, I.; Yli-Juuti, T.; Pierce, J. R.; Petaja, T.; Worsnop, D. R.; Kulmala, M.; Donahue, N. M. *Nat. Geosci.* **2012**, *5*, 453−458.
(15) Kuang, C.; McMurry, P. H.; McCormick, A. V.; Eisele, F. L. *J. Geophys. Res.: Atmos.* **2008**, *113*, D10209.
(16) Nieminen, T.; Manninen, H. E.; Sihto, S. L.; Yli-Juuti, T.; Mauldin, R. L.; Petaja, T.; Riipinen, I.; Kerminen, V. M.; Kulmala, M. *Environ. Sci. Technol.* **2009**, *43*, 4715−4721.
(17) Sipila, M.; Berndt, T.; Petaja, T.; Brus, D.; Vanhanen, J.; Stratmann, F.; Patokoski, J.; Mauldin, R. L.; Hyvarinen, A. P.; Lihavainen, H.; Kulmala, M. *Science* **2010**, *327*, 1243−1246.
(18) Weber, R. J.; Marti, J. J.; McMurry, P. H.; Eisele, F. L.; Tanner, D. J.; Jefferson, A. *Chem. Eng. Commun.* **1996**, *151*, 53−64.
(19) Weber, R. J.; Marti, J. J.; McMurry, P. H.; Eisele, F. L.; Tanner, D. J.; Jefferson, A. *J. Geophys. Res.: Atmos.* **1997**, *102*, 4375−4385.
(20) Bzdek, B. R.; Zordan, C. A.; Pennington, M. R.; Luther, G. W.; Johnston, M. V. *Environ. Sci. Technol.* **2012**, *46*, 4365−4373.
(21) Kuang, C.; Chen, M.; Zhao, J.; Smith, J.; McMurry, P. H.; Wang, J. *Atmos. Chem. Phys.* **2012**, *12*, 3573−3589.
(22) Kuang, C.; Riipinen, I.; Sihto, S. L.; Kulmala, M.; McCormick, A. V.; McMurry, P. H. *Atmos. Chem. Phys.* **2010**, *10*, 8469−8480.
(23) Smith, J. N.; Barsanti, K. C.; Friedli, H. R.; Ehn, M.; Kulmala, M.; Collins, D. R.; Scheckman, J. H.; Williams, B. J.; McMurry, P. H. *Proc. Natl. Acad. Sci. U.S.A.* **2010**, *107*, 6634−6639.
(24) Smith, J. N.; Dunn, M. J.; VanReken, T. M.; Iida, K.; Stolzenburg, M. R.; McMurry, P. H.; Huey, L. G. *Geophys. Res. Lett.* **2008**, *35*, L04808.
(25) Stolzenburg, M. R.; McMurry, P. H.; Sakurai, H.; Smith, J. N.; Mauldin, R. L.; Eisele, F. L.; Clement, C. F. *J. Geophys. Res.: Atmos.* **2005**, *110*, D22s05.
(26) Berndt, T.; Stratmann, F.; Sipila, M.; Vanhanen, J.; Petaja, T.; Mikkila, J.; Gruner, A.; Spindler, G.; Mauldin, R. L.; Curtius, J.; Kulmala, M.; Heintzenberg, J. *Atmos. Chem. Phys.* **2010**, *10*, 7101−7116.
(27) Kirkby, J.; Curtius, J.; Almeida, J.; Dunne, E.; Duplissy, J.; Ehrhart, S.; Franchin, A.; Gagne, S.; Ickes, L.; Kurten, A.; Kupc, A.; Metzger, A.; Riccobono, F.; Rondo, L.; Schobesberger, S.; Tsagkogeorgas, G.; Wimmer, D.; Amorim, A.; Bianchi, F.; Breitenlechner, M.; David, A.; Dommen, J.; Downard, A.; Ehn, M.; Flagan, R. C.; Haider, S.; Hansel, A.; Hauser, D.; Jud, W.; Junninen, H.; Kreissl, F.; Kvashin, A.; Laaksonen, A.; Lehtipalo, K.; Lima, J.; Lovejoy, E. R.; Makhmutov, V.; Mathot, S.; Mikkila, J.; Minginette, P.; Mogo, S.; Nieminen, T.; Onnela, A.; Pereira, P.; Petaja, T.; Schnitzhofer, R.; Seinfeld, J. H.; Sipila, M.; Stozhkov, Y.; Stratmann, F.; Tome, A.; Vanhanen, J.; Viisanen, Y.; Vrtala, A.; Wagner, P. E.; Walther, H.; Weingartner, E.; Wex, H.; Winkler, P. M.; Carslaw, K. S.; Worsnop, D. R.; Baltensperger, U.; Kulmala, M. *Nature* **2011**, *476*, 429−433.
(28) Kurten, T.; Loukonen, V.; Vehkamaki, H.; Kulmala, M. *Atmos. Chem. Phys.* **2008**, *8*, 4095−4103.
(29) Ortega, I. K.; Kurten, T.; Vehkamaki, H.; Kulmala, M. *Atmos. Chem. Phys.* **2009**, *9*, 7431−7434.
(30) Yu, H.; McGraw, R.; Lee, S. H. *Geophys. Res. Lett.* **2012**, *39*, L02807.
(31) Zollner, J. H.; Glasoe, W. A.; Panta, B.; Carlson, K. K.; McMurry, P. H.; Hanson, D. R. *Atmos. Chem. Phys.* **2012**, *12*, 4399−4411.
(32) Nadykto, A. B.; Yu, F. Q.; Jakovleva, M. V.; Herb, J.; Xu, Y. S. *Entropy* **2011**, *13*, 554−569.
(33) Ehn, M.; Junninen, H.; Petaja, T.; Kurten, T.; Kerminen, V. M.; Schobesberger, S.; Manninen, H. E.; Ortega, I. K.; Vehkamaki, H.; Kulmala, M.; Worsnop, D. R. *Atmos. Chem. Phys.* **2010**, *10*, 8513−8530.
(34) Petaja, T.; Sipila, M.; Paasonen, P.; Nieminen, T.; Kurten, T.; Ortega, I. K.; Stratmann, F.; Vehkamaki, H.; Berndt, T.; Kulmala, M. *Phys. Rev. Lett.* **2011**, *106*, 228302.
(35) Young, L. H.; Benson, D. R.; Kameel, F. R.; Pierce, J. R.; Junninen, H.; Kulmala, M.; Lee, S. H. *Atmos. Chem. Phys.* **2008**, *8*, 4997−5016.
(36) Eisele, F. L.; Lovejoy, E. R.; Kosciuch, E.; Moore, K. F.; Mauldin, R. L.; Smith, J. N.; McMurry, P. H.; Iida, K. *J. Geophys. Res.: Atmos.* **2006**, *111*, D04305.
(37) Ball, S. M.; Hanson, D. R.; Eisele, F. L.; McMurry, P. H. *J. Geophys. Res.: Atmos.* **1999**, *104*, 23709−23718.
(38) Benson, D. R.; Yu, J. H.; Markovich, A.; Lee, S. H. *Atmos. Chem. Phys.* **2011**, *11*, 4755−4766.
(39) Hanson, D. R.; Eisele, F. L. *J. Geophys. Res.: Atmos.* **2002**, *107*, 4158.
(40) Korhonen, P.; Kulmala, M.; Laaksonen, A.; Viisanen, Y.; McGraw, R.; Seinfeld, J. H. *J. Geophys. Res.: Atmos.* **1999**, *104*, 26349−26353.
(41) Zhao, J.; Smith, J. N.; Eisele, F. L.; Chen, M.; Kuang, C.; McMurry, P. H. *Atmos. Chem. Phys.* **2011**, *11*, 10823−10836.
(42) Anderson, K. E.; Siepmann, J. I.; McMurry, P. H.; VandeVondele, J. *J. Am. Chem. Soc.* **2008**, *130*, 14144−14147.
(43) Dawson, M. L.; Varner, M. E.; Perraud, V.; Ezell, M. J.; Gerber, R. B.; Finlayson-Pitts, B. J. *Proc. Natl. Acad. Sci. U.S.A.* **2012**, *109*, 18719−18724.
(44) Metzger, A.; Verheggen, B.; Dommen, J.; Duplissy, J.; Prevot, A. S. H.; Weingartner, E.; Riipinen, I.; Kulmala, M.; Spracklen, D. V.; Carslaw, K. S.; Baltensperger, U. *Proc. Natl. Acad. Sci. U.S.A.* **2010**, *107*, 6646−6651.
(45) Zhang, R. Y.; Suh, I.; Zhao, J.; Zhang, D.; Fortner, E. C.; Tie, X. X.; Molina, L. T.; Molina, M. J. *Science* **2004**, *304*, 1487−1490.
(46) Zhang, R. Y.; Wang, L.; Khalizov, A. F.; Zhao, J.; Zheng, J.; McGraw, R. L.; Molina, L. T. *Proc. Natl. Acad. Sci. U.S.A.* **2009**, *106*, 17650−17654.
(47) Riipinen, I.; Sihto, S. L.; Kulmala, M.; Arnold, F.; Dal Maso, M.; Birmili, W.; Saarnio, K.; Teinila, K.; Kerminen, V. M.; Laaksonen, A.; Lehtinen, K. E. J. *Atmos. Chem. Phys.* **2007**, *7*, 1899−1914.
(48) Curtius, J.; Froyd, K. D.; Lovejoy, E. R. *J. Phys. Chem. A* **2001**, *105*, 10867−10873.
(49) Froyd, K. D.; Lovejoy, E. R. *J. Phys. Chem. A* **2003**, *107*, 9800−9811.
(50) Froyd, K. D.; Lovejoy, E. R. *J. Phys. Chem. A* **2003**, *107*, 9812−9824.
(51) Froyd, K. D.; Lovejoy, E. R. *J. Phys. Chem. A* **2012**, *116*, 5886−5899.
(52) Lovejoy, E. R.; Curtius, J. *J. Phys. Chem. A* **2001**, *105*, 10874−10883.
(53) Sorokin, A.; Arnold, F.; Wiedner, D. *Atmos. Environ.* **2006**, *40*, 2030−2045.
(54) Bzdek, B. R.; Ridge, D. P.; Johnston, M. V. *Atmos. Chem. Phys.* **2010**, *10*, 3495−3503.
(55) Bzdek, B. R.; Ridge, D. P.; Johnston, M. V. *J. Phys. Chem. A* **2010**, *114*, 11638−11644.
(56) Bzdek, B. R.; Ridge, D. P.; Johnston, M. V. *J. Geophys. Res.: Atmos.* **2011**, *116*, D03301.
(57) Bzdek, B. R.; Ridge, D. P.; Johnston, M. V. *Atmos. Chem. Phys.* **2011**, *11*, 8735−8743.
(58) DePalma, J. W.; Bzdek, B. R.; Doren, D. J.; Johnston, M. V. *J. Phys. Chem. A* **2012**, *116*, 1030−1040.
(59) Laskin, J.; Denisov, E. V.; Shukla, A. K.; Barlow, S. E.; Futrell, J. H. *Anal. Chem.* **2002**, *74*, 3255−3261.
(60) Laskin, J.; Byrd, M.; Futrell, J. *Int. J. Mass Spectrom.* **2000**, *195*, 285−302.

(61) Laskin, J.; Futrell, J. *J. Phys. Chem. A* **2000**, *104*, 5484−5494.
(62) Shaffer, S. A.; Tang, K. Q.; Anderson, G. A.; Prior, D. C.; Udseth, H. R.; Smith, R. D. *Rapid Commun. Mass Spectrom.* **1997**, *11*, 1813−1817.
(63) Mize, T. H.; Taban, I.; Duursma, M.; Seynen, M.; Konijnenburg, M.; Vijftigschild, A.; Doornik, C. V.; Rooij, G. V.; Heeren, R. M. A. *Int. J. Mass Spectrom.* **2004**, *235*, 243−253.
(64) Taban, L. M.; van der Burgt, Y. E. M.; Duursma, M.; Takats, Z.; Seynen, M.; Konijnenburg, M.; Vijftigschild, A.; Attema, I.; Heeren, R. M. A. *Rapid Commun. Mass Spectrom.* **2008**, *22*, 1245−1256.
(65) Dunbar, R. C. *Mass Spectrom. Rev.* **1992**, *11*, 309−339.
(66) Laskin, J.; Denisov, E.; Futrell, J. *J. Am. Chem. Soc.* **2000**, *122*, 9703−9714.
(67) Laskin, J. *J. Phys. Chem. A* **2006**, *110*, 8554−8562.
(68) Laskin, J.; Yang, Z.; Song, T.; Lam, C.; Chu, I. K. *J. Am. Chem. Soc.* **2010**, *132*, 16006−16016.
(69) Dewar, M. J. S.; Zoebisch, E. G.; Healy, E. F.; Stewart, J. J. P. *J. Am. Chem. Soc.* **1985**, *107*, 3902−3909.
(70) *HyperChem Professional 8.0.8*; Hypercube, Inc.: Gainesville, FL, 2010.
(71) Perdew, J. P.; Burke, K.; Wang, Y. *Phys. Rev. B* **1996**, *54*, 16533−16539.
(72) Perdew, J. P.; Chevary, J. A.; Vosko, S. H.; Jackson, K. A.; Pederson, M. R.; Singh, D. J.; Fiolhais, C. *Phys. Rev. B* **1992**, *46*, 6671−6687.
(73) Frisch, M. J.; Trucks, G. W.; Schlegel, H. B.; Scuseria, G. E.; Robb, M. A.; Cheeseman, J. R.; Scalmani, G.; Barone, V.; Mennucci, B.; Petersson, G. A.; Nakatsuji, H.; Caricato, M.; Li, X.; Hratchian, H. P.; Izmaylov, A. F.; Bloino, J.; Zheng, G.; Sonnenberg, J. L.; Hada, M.; Ehara, M.; Toyota, K.; Fukuda, R.; Hasegawa, J.; Ishida, M.; Nakajima, T.; Honda, Y.; Kitao, O.; Naka, H.; Vreven, T.; Montgomery, J. A.; Peralta, J. E.; Ogliaro, F.; Bearpark, M.; Heyd, J. J.; Brothers, E.; Kudin, K. N.; Staroverov, V. N.; Keith, T.; Kobayashi, R.; Normand, J.; Raghavachari, K.; Rendell, A.; Burant, J. C.; Iyengar, S. S.; Tomasi, J.; Cossi, M.; Rega, N.; Millam, J. M.; Klene, M.; Knox, J. E.; Cross, J. B.; Bakken, V.; Adamo, C.; Jaramillo, J.; Gomperts, R.; Stratmann, R. E.; Yazyev, O.; Austin, A. J.; Cammi, R.; Pomelli, C.; Ochterski, J. W.; Martin, R. L.; Morokuma, K.; Zakrzewski, V. G.; Voth, G. A.; Salvador, P.; Dannenberg, J. J.; Dapprich, S.; Daniels, A. D.; Farkas, O.; Foresman, J. B.; Ortiz, J. V.; Cioslowski, J.; Fox, D. J. *Gaussian 09*, revision C.01; Gaussian, Inc.: Wallingford, CT, 2010.
(74) Moller, C.; Plesset, M. S. *Phys. Rev.* **1934**, *46*, 0618−0622.
(75) Dunning, T. H. *J. Chem. Phys.* **1989**, *90*, 1007−1023.
(76) Zhou, M.; Huang, C.; Wysocki, V. H. *Anal. Chem.* **2012**, *84*, 6016−6023.
(77) Wysocki, V. H.; Jones, C. M.; Galhena, A. S.; Blackwell, A. E. *J. Am. Soc. Mass Spectrom.* **2008**, *19*, 903−913.
(78) Kurten, T.; Kuang, C. A.; Gomez, P.; McMurry, P. H.; Vehkamaki, H.; Ortega, I.; Noppel, M.; Kulmala, M. *J. Chem. Phys.* **2010**, *132*, 024304.
(79) Kurten, T.; Petaja, T.; Smith, J.; Ortega, I. K.; Sipila, M.; Junninen, H.; Ehn, M.; Vehkamaki, H.; Mauldin, L.; Worsnop, D. R.; Kulmala, M. *Atmos. Chem. Phys.* **2011**, *11*, 3007−3019.
(80) Finlayson-Pitts, B. J.; Pitts, J. N. *Chemistry of the Upper and Lower Atmosphere*; Academic Press: New York, 2000.
(81) McGrath, M. J.; Olenius, T.; Ortega, I. K.; Loukonen, V.; Paasonen, P.; Kurten, T.; Kulmala, M.; Vehkamaki, H. *Atmos. Chem. Phys.* **2012**, *12*, 2345−2355.
(82) Kulmala, M. *Atmos. Res.* **2010**, *98*, 201−206.
(83) Chen, M.; Titcombe, M.; Jiang, J.; Jen, C.; Kuang, C.; Fischer, M. L.; Eisele, F. L.; Siepmann, J. I.; Hanson, D. R.; Zhao, J.; McMurry, P. H. *Proc. Natl. Acad. Sci. U.S.A.* **2012**, *109*, 18713−18718.